

# Simultaneous Myoelectric Control of a Robot Arm using Muscle Synergy-Inspired Inputs from High-Density Electrode Grids

Mark Ison, Ivan Vujaklija, Bryan Whitsell, Dario Farina and Panagiotis Artemiadis

**Abstract**—Myoelectric control has seen decades of research as a potential interface between human and machines. High-density surface electromyography (HDsEMG) non-invasively provides a rich set of signals representing underlying muscle contractions and, at a higher level, human motion intent. Many pattern recognition techniques have been proposed to predict motions based on these signals. However, control schemes incorporating pattern recognition struggle with long-term reliability due to signal stochasticity and transient changes. This study proposes an alternative approach for HDsEMG-based interfaces using concepts of motor skill learning and muscle synergies to address long-term reliability. Muscle synergy-inspired decomposition reduces HDsEMG into control inputs robust to small electrode displacements. The novel control scheme provides simultaneous and proportional control, and is learned by the subject simply by interacting with the device. In a multiple-day experiment, subjects learned to control a virtual 7-DoF myoelectric interface, displaying performance learning curves consistent with motor skill learning. On a separate day, subjects intuitively transferred this learning to demonstrate precision tasks with a 7-DoF robot arm, without requiring any recalibration. These results suggest that the proposed method may be a practical alternative to pattern recognition-based control for long-term use of myoelectric interfaces.

## I. INTRODUCTION

Myoelectric control, with potential to manipulate multiple degrees-of-freedom (DoFs) simultaneously via muscle activity [1], offers a convenient interface between humans and machines, most notably in functional prostheses [2] and robot teleoperation [3]. HDsEMG records a complete set of muscle activity without requiring exact placement over the desired muscles, and has been used in conjunction with pattern recognition techniques to generate simultaneous myoelectric control schemes [4]–[6]. However, these specific control schemes depend on a user’s motion repeatability and a training set of signals used to generate predicted outputs, both of which are unreliable due to signal stochasticity and transient changes over time [1]. Thus, state-of-the-art myoelectric control schemes struggle to provide reliable long-term simultaneous control, which has limited the commercial success of myoelectric interfaces [7].

This study was financially supported by the European Research Council (ERC) via the ERC Advanced Grant DEMOVE (No. 267888). All authors declare no conflict of interests

M. Ison, B. Whitsell, and P. Artemiadis are with the School for Engineering of Matter, Transport and Energy, Arizona State University, Tempe, AZ 85287-6106 USA (e-mail: panagiotis.artemiadis@asu.edu).

I. Vujaklija and D. Farina are with the Department of Neurorehabilitation Engineering, Bernstein Focus Neurotechnology Göttingen, Bernstein Center for Computational Neuroscience, University Medical Center Göttingen, Georg-August University, 37075 Göttingen, Germany (e-mail: dario.farina@bccn.uni-goettingen.de).

On the other hand, recent works have shown that users adapt to myoelectric controls, regardless of their relationship to normal kinematics, to improve control capabilities over time when given visual feedback [8], [9]. Ison and Artemiadis related these adaptations to typical motor skill learning, resulting in performance retention, generalization, and transfer for efficient control of myoelectric interfaces [10], [11]. While these approaches demonstrate robust long-term control, they rely on targeted muscles to avoid biomechanical constraints, limiting them to control of a few DoFs [12]–[15].

This paper proposes a novel method for robust long-term control of myoelectric interfaces using HDsEMG and a control scheme based on concepts of motor skill learning and muscle synergies. HDsEMG avoids the need of targeted electrode placement required in previous motor learning-based control schemes while maintaining long-term control characteristics associated with learning new motor skills [15], [16]. The developed scheme decomposes the incoming signals into robust muscle synergy-inspired inputs with intention to control a 7-DoF robotic arm and hand (Cartesian position and orientation, plus hand grasping). A two-state finite state machine allows 4-DoFs to be controlled simultaneously, with a switching method to change the control state between position and orientation for full articulation of all 7-DoFs. To the best of the authors’ knowledge, no other work has demonstrated real-time control of a 7-DoF myoelectric interface offering both session-independence and simultaneous control from untargeted muscles.

The control scheme is learned by subjects as they interact with a virtual reality (VR) interface over two days. Throughout the two sessions, subjects display motor learning trends consistent with previous works controlling fewer DoFs with targeted muscles [10], [12], [13]. Between one and eight days later, subjects test their capability to perform centimeter-precision tasks with the 7-DoF robot arm and hand using the same control scheme. Despite noticeable differences in system dynamics due to physical constraints such as joint limits and inertia, subjects naturally transferred their learning to operate the robot with a sense of intuitiveness. This result supports the proposed method as a viable alternative for myoelectric interfaces designed for long-term use.

## II. METHODS

The three-session experiment was designed to explore and measure performance of a new control paradigm for a 7-DoF myoelectric interface. Each subject learned a novel, customized mapping over two sessions by interacting with a VR interface. One to eight days later, subjects returned to

perform a series of precision tasks, using a 7-DoF KUKA Light Weight Robot 4 (LWR 4) with a Touch Bionics iLIMB Ultra robotic hand attached.

### A. Control Paradigm

The proposed control algorithm was engineered to provide stable output using the rich set of information obtained from high density (HD) electrode grids. The large number of observations are reduced to a small set of robust inputs using a muscle synergy-inspired dimensionality reduction. Namely, the underlying model presented by Jiang et. al [17] states that sEMG recordings,  $\mathbf{Y}(t)$  can be interpreted as instantaneous mixtures of muscle activation signals,  $\mathbf{F}(t)$ . Muceli et. al [18] represent this relationship as:

$$\mathbf{Y}(t) = \mathbf{W} \cdot \mathbf{F}(t) \quad (1)$$

with  $\mathbf{W}$  a matrix of channel weights indicating the contribution of the  $m$  activation signals to each of the  $n$  electrodes. Its columns,  $\mathbf{W}_i$ ,  $i \in \{1..m\}$ , approximate a user's muscle synergies in the form of a high-level input [1].  $\mathbf{W}$  is obtained using the DoF-wise non-negative matrix factorization (NMF) algorithm as described in [17]. Due to NMF's intrinsic properties,  $k < m$  robust, quasi-independent activation signals are extracted by approximating a subset of  $k$  independent columns in  $\mathbf{W}$ , resulting in an  $n \times k$  semi-orthogonal matrix,  $\hat{\mathbf{W}}$ . The algorithm generating  $\hat{\mathbf{W}}$  is as follows, where  $\mathbf{G}$  is a  $4 \times 4$  Gaussian kernel,  $\mathbf{A} * \mathbf{B}$  is the 2D convolution of  $\mathbf{A}$  and  $\mathbf{B}$ , and  $\delta(\mathbf{V})$  thresholds  $\mathbf{V}$  to zero at one standard deviation below the largest element of  $\mathbf{V}$ :

- 1) Reshape each  $\mathbf{W}_i$  according to the 2D configuration of the HD electrode grid.
- 2) For each  $\mathbf{W}_i$ :  $\mathbf{W}'_i = \delta(\mathbf{W}_i) * \mathbf{G}$
- 3) Merge  $\mathbf{W}'_a$  and  $\mathbf{W}'_b$ , where  $\mathbf{W}'_a$  and  $\mathbf{W}'_b$  have the closest cosine similarity of all  $\mathbf{W}'_i$  pairs.
- 4) Repeat step 3 until only  $k$  matrices remain in  $\mathbf{W}'$ .
- 5) For each remaining  $\mathbf{W}'_i$ :  $\mathbf{W}''_i = \delta(\mathbf{W}'_i) * \mathbf{G}$
- 6) For each  $\mathbf{W}''_i$ :  $\hat{\mathbf{W}}_i = \frac{\mathbf{W}''_i}{|\mathbf{W}''_i|}$ , reshaped to a row vector

The semi-orthogonality of  $\hat{\mathbf{W}}$  guarantees that the left inverse,  $\hat{\mathbf{W}}_{left}^{-1}$ , exists, and is simply the transpose,  $\hat{\mathbf{W}}^T$ . Thus, (1) can be rearranged to decompose HDsEMG into quasi-independent control inputs,  $\hat{\mathbf{F}}(t)$ , approximating activation signals  $\mathbf{F}(t)$ :

$$\hat{\mathbf{F}}(t) = \hat{\mathbf{W}}^T \cdot \mathbf{Y}(t) \quad (2)$$

$\hat{\mathbf{W}}$  is initially calibrated using linear envelopes [19] extracted from  $n$  HDsEMG channels. A randomized linear mapping is adapted from [10], transforming  $n$  linear envelopes of sEMG,  $\mathbf{Y}(t)$ , to  $c$  control outputs,  $\mathbf{U}(t)$ :

$$\mathbf{U}(t) = g\mathbf{M}\hat{\mathbf{W}}^T [(\mathbf{Y}(t) - \sigma) \circ u(\mathbf{Y}(t) - \sigma)], \quad (3)$$

where  $\circ$  is an element-wise matrix multiplication,  $u(*)$  is the unit step function,  $\sigma$  is the muscle activation threshold, and  $g$  is the output gain. Both  $\sigma$  and  $g$  can be tuned for each subject, and  $\mathbf{M}$  is a semi-random mixing matrix converting  $\hat{\mathbf{F}}(t)$  to the control outputs  $\mathbf{U}(t)$ .  $\mathbf{U}(t)$  is averaged over the last five outputs to provide consistent control.

TABLE I  
FINITE STATE MACHINE CONTROL AXES

Control Axis	Position State	Orientation State
1	X	Yaw ( $\phi$ )
2	Y	Pitch ( $\theta$ )
3	Z	Roll ( $\rho$ )
4	Color (Virtual) or Hand Open/Close (Robot)	

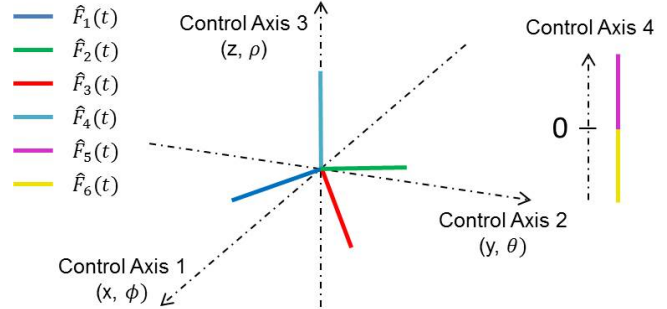


Fig. 1. Visualization of mapping  $\mathbf{M}$ , transforming control inputs  $\hat{\mathbf{F}}(t)$  to four output control axes  $\mathbf{U}(t)$ , where each axis is as defined in Table I.

In this experiment, the 7-DoF control scheme is implemented as a two-state finite state machine (FSM), with each state offering simultaneous control of velocities over 4-DoFs (see Table I).  $\mathbf{M}$  is designed to cover the entire output space ( $c = 4$ ) using minimal inputs ( $k = 6$ ) while decoupling control axes 1-3 from control axis 4 (see Fig. 1):

$$\mathbf{M} = \begin{bmatrix} 0.52 & -0.94 & 0.42 & 0.00 & 0.00 & 0.00 \\ 0.79 & 0.06 & -0.85 & 0.00 & 0.00 & 0.00 \\ -0.33 & -0.34 & -0.33 & 1.00 & 0.00 & 0.00 \\ 0.00 & 0.00 & 0.00 & 0.00 & 1.00 & -1.00 \end{bmatrix} \quad (4)$$

State switching is done by monitoring the simultaneous threshold breach between the last two activation inputs,  $\hat{F}_5$  and  $\hat{F}_6$ , contributed by an antagonistic muscle pair.

1) *Pre-Processing*: The HDsEMG signals are subtracted from the mean of all channels to dampen the influence of common noise, and then rectified and low-pass filtered (fourth-order zero-lag Butterworth, cut-off 3Hz). Finally, the signals are filtered by a 3x3 median filter to minimize the effects of electrode lift-off. The sEMG signals of an additional antagonistic muscle pair are rectified, low-pass filtered (fourth-order zero-lag Butterworth, cut-off 3Hz), and normalized with respect to the subject's maximal voluntary contraction (MVC) for these two muscles, as found during the initial calibration. Both series of signals are then sub-sampled to 200Hz and merged to create  $\mathbf{Y}(t)$ .

2) *Calibration*: Each subject is first guided through the calibration stage described in [20] to generate a unique  $\mathbf{W}$ . A total of 16 wrist and finger motions from the right arm are investigated - wrist flexion/extension, wrist pronation/supination, ulnar/radial deviation, hand open/close and flexion/extension of the index, middle, ring, and pinky fingers. 192 HDsEMG signals are collected from the subject's forearm using HD electrode grids to form an initial  $\hat{\mathbf{W}}_0$  with  $k_0 = 4$ . Two additional columns are added with unit input on the 193<sup>rd</sup> and 194<sup>th</sup> rows, respectively, and zeros elsewhere.



Fig. 2. VR control setup including the sEMG systems and monitor.

These two columns contain the sEMG from biceps brachii (BB) and triceps brachii (TB), resulting in a  $194 \times 6$  matrix  $\tilde{\mathbf{W}}$ . During this calibration phase, subjects are also asked to perform their MVC for BB and TB to initially set the state switching threshold at 50% of it. MVC values are *not* needed from the HDsEMG, as explained in [10].

3) *Robot Control*: There is a slight difference in operation between VR and robot control induced by joint limits, singularities, and inertia. LWR 4 operates in Cartesian impedance control using inverse kinematics when the control state is in position, and joint impedance control using forward kinematics of the three wrist joints when the control state is in orientation mode. The switch is enforced to reduce the risk of joint velocity and position limits being exceeded while rotating through singularities. Global  $\rho$ ,  $\phi$ , and  $\theta$  are limited to  $\pm \frac{\pi}{3}$  radians to avoid physical limitations while rotating. The iLIMB operates via Bluetooth with velocity commands sent to open/close all fingers at  $200Hz$ .

### B. Experimental Setup

Two sEMG systems were used for data collection. The first system included 192 monopolar channels from the subject's forearm using three equidistant semi-disposable adhesive  $8 \times 8$  grids with  $10mm$  inter-electrode distance. The EMG-USB2, OT Bioelettronica amplifier was set to gain of 1000 with internal bandpass filter at  $3 - 900Hz$ , broadcasting samples via TCP at  $2048Hz$  with 12-bit depth for further processing, as in [18]. The second system included two bipolar channels placed on the BB and TB muscles. These wireless sEMG electrodes (Delsys Trigno Wireless) were acquired with a gain of 500, digitized with 16-bit depth at a frequency of  $1926Hz$  and broadcast via TCP. Both interfaces receive commands at  $200Hz$  from a custom program using C++ and OpenGL API [21]. This program performs real-time processing and conversion of sEMG inputs into control variables of linear velocity, angular velocity and color/grasp. The full setups are shown in Fig. 2 and 3, respectively.

### C. Experimental Protocol

Subjects, without prior knowledge on how to control the interface, attended three sessions across several days. The first session consisted of the calibration phase described above, followed by an introductory control phase. The control phase introduced subjects to the VR helicopter, with 20 minutes of exploration, in which the subject was encouraged



Fig. 3. Robot control setup including the sEMG systems, LWR 4, iLIMB, and three target objects to grasp and move to the bin.

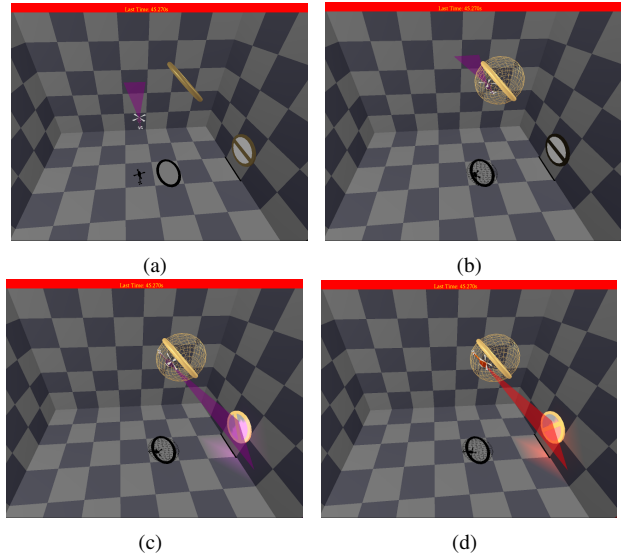


Fig. 4. Subtask sequence in VR. The helicopter starts from the initial configuration (a), moves using position state control to the center of the ring (b), switches to orientation state and aligns with the target on the wall (c), and finally matches the color, representing the grasp control, of the top panel (d). Note that the color task can be completed simultaneously, but the position and orientation task must be completed in order.

to explore the space and become familiar with the control paradigm, followed by 26 tasks to be completed. The tasks are distributed as to cover the entire volume of the task-space and require activation of all available DoFs, as explained in Fig. 4. After completing each full task, the helicopter returns to the center of the screen with an initial orientation and color followed by a ten second break. There was no time limit imposed in order to encourage users to explore and discover a comfortable control. The random arrangement of targets was consistent for each subject in the experiment.

The second session occurred at least 24 hours after the first. Subjects were given one hour to accomplish as many tasks as possible while using the same control scheme and  $\tilde{\mathbf{W}}$  calculated during the first session. This session provided data regarding learning retention and continued learning trends.

The final session occurred between one and eight days after the second. Subjects were introduced to the robot myoelectric interface, while using the same control scheme and  $\tilde{\mathbf{W}}$  calculated in session one. Subjects are asked to complete three precision tasks, with no strict order, by sequentially grasping a tennis-sized ball and two customized clothespins



Fig. 5. Subtask sequence for the robot interface. The robot hand is controlled to grasp two clothespins and a ball. Each object is arranged such that the hand must change both position and orientation to grasp the object. The object is then placed into the bin below the table. The order in which these tasks are completed is determined by each subject. The clothespins must be grasped as shown in the images to successfully complete the task.

TABLE II  
EVALUATION METRICS

Metric	Linear Learning Fit
Completion Time ( $CT$ )	$CT(b) = \kappa_{ct} - \beta_{ct}b$
Throughput ( $TP$ )	$TP(b) = \kappa_{tp} + \beta_{tp}b$
Path Efficiency ( $PE$ )	$PE(b) = \kappa_{pe} + \beta_{pe}b$

to place in a bin. The task sequence is timed and shown in Fig. 5. This session provided evidence of precision control capabilities and learning transfer despite slightly different system dynamics of the robot compared to the VR.

#### D. Data Analysis

During the first two sessions, collected datasets contained values describing task difficulty, completion times, and path lengths used to accomplish each task. This data was analyzed in data blocks containing 25% of each session’s data from all subjects. The total completion time is recorded for the third session to indicate precision performance capabilities and any factors influencing these capabilities.

1) *Learning Trends*: Metrics used for assessing performance in the first two sessions are provided in Table II, using first degree polynomials to fit the results with respect to block number. These linear trends are assumed according to [10], as the initial exponential learning component has been accounted for in the first 20 minutes of exploration.

$CT$  is the time needed to fulfill the task [22].  $TP$ , expressed in bits/second according to Fitts’ law [23], measures both speed and accuracy by considering the difficulty of the task [9].  $PE$  is the ratio between the shortest path possible to complete the entire task and the actual path taken to reach the target [24].  $b$  is the overall block number in session 1 and 2,  $\kappa$  is initial performance, and  $\beta$  shows the learning rate, such that  $\beta > 0$  indicates better performance and a significant learning component, for each metric.

The index of difficulty,  $ID$ , of a given task is given by the Shannon Formulation [23]:

$$ID = \log_2\left(\frac{D}{W_D} + 1\right) \quad (5)$$

where  $W_D$  is the combined error tolerance of all targets (held constant throughout this experiment), and  $D$  is the optimal distance needed to complete the task:

$$D = \frac{1}{g}(0.471\gamma_1 + \gamma_2) \quad (6)$$

with  $\gamma_1$  as the straight line distance from the starting position to the center of the ring, and  $\gamma_2$  as the angular distance between the starting orientation of the helicopter and the target orientation, with respect to vectors originating at the center of the ring.  $\gamma_1$  is normalized by the ratio between the output linear velocity in position state and output angular velocity in orientation state when given unit input  $\hat{\mathbf{F}}(t)$ .  $TP$  is then calculated as:

$$TP = \frac{ID}{CT}. \quad (7)$$

2) *Robot Control*: Subjects qualitatively demonstrate their control capabilities by completing precision tasks in the third session. This performance is influenced by a vast number of immeasurable factors (strategy, understanding of physical constraints on the joints, etc.). Other factors, such as performance in the virtual tasks, time between session two and three, and the choice of  $\hat{\mathbf{W}}$ , are quantified and ranked based on correlation with the total time needed by each subject to complete the precision tasks.

To establish a baseline completion time for this set of tasks, the same subjects returned to perform the same tasks with more conventional, noiseless keyboard inputs generating  $\hat{\mathbf{F}}(t)$ . Subjects were given 10 minutes to practice controlling the robot, learn the physical constraints, and develop a strategy for completing the tasks. The subjects then completed the same three precision tasks as previously done with sEMG.

### III. RESULTS

In total, eight healthy subjects (all male, age 19-40, 1 left handed, 7 right handed) participated in the experiment upon signing the informed consent according to the procedures approved by the ASU IRB (Protocol: #1201007252). Potential outlier behavior was observed in two subjects. One subject experienced sudden confusion during the second session (block 6) which caused a loss of control and led to tension as he struggled to recover prior performance. On the other hand, a different participant nearly mastered the controls during the exploratory 20 minutes, and displayed minimal learning throughout the rest of the sessions. Both subjects are included in all presented results, with the influence of the former most visible at the analysis of block 6.

#### A. Learning Trends

On average, subjects had 30 hours between session one and two, and all but one reported control to be easier during the start of the second session despite having no exploration

TABLE III  
LEARNING TRENDS FITTING PARAMETERS

Metric	$\beta$	$\beta$ [95% CI]	$\kappa$	$R^2$
$CT(b)$	17.10	[12.40, 21.70]	177.0	0.94
$TP(b)$	0.023	[0.019, 0.028]	0.06	0.98
$PE(b)$	0.031	[0.024, 0.038]	0.20	0.10

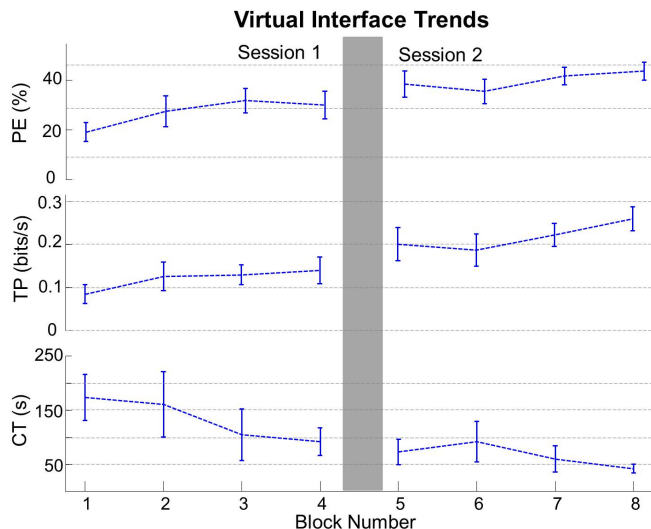


Fig. 6. VR performance metrics as functions of block numbers across all subjects. Each metric shows a significant and consistent learning rate regardless of the break between sessions. Error bars represent 95% confidence intervals within each block.

time and potential electrode shifts between sessions. The mean values of  $CT$ ,  $TP$  and  $PE$  within each block were fit to Table II, with parameter values presented in Table III.

Table III reveals a significant learning rate for each of  $CT$ ,  $TP$  and  $PE$ , visualized in Fig. 6. Despite the non-intuitive control scheme resulting in initial poor performance, subjects consistently improve their performance metrics, even after beginning a new session. Both  $CT$  and  $TP$  have strong linear fits, while  $PE$  has a poorer fit, which is expected due to the bias toward higher variance as the mean path efficiency increases [10]. As shown by the differences between blocks 4 and 5 in Fig. 6, all subjects were able to maintain consistent learning despite the break between sessions. Note that the inconsistency in block 6 is caused by one subject suddenly experiencing confusion.

### B. Robot Control

Subjects had an average of 97 hours ( $\sim 4$  days) between session two and three. Again, all but one subject found controls consistent during the start of the third session. However, all subjects reported occasional delays in the control outputs, which were actually caused by generating outputs exceeding physical joint and velocity limits. An example task sequence is shown in Fig. 7. A supplementary video demonstrating the various precision tasks is available at:

<https://www.youtube.com/watch?v=Qre134jA4TQ>.

The relationship between the robot task completion time and identified sources of influence are considered by corre-

TABLE IV  
INFLUENTIAL FACTORS IN ROBOT COMPLETION TIME

Factor	Correlation (R)
Throughput	-0.82
Completion Time	+0.70
Path Efficiency	-0.61
Delay	-0.16
$\hat{W}$	+0.37

lation coefficients between the metrics for each subject, displayed in Table IV. The only significant correlation observed is with throughput from the end of session two. Completion time and path efficiency at the end of session two are moderately correlated, while the weak negative correlation with delay suggests that performance degradation is not a significant factor in the robot control.

$\hat{W}$  is considered using cosine similarity to the subject with significantly better control than any other subject (robot task completion time was only 6 minutes) to determine if the choice of  $\hat{W}$  may have influenced the performance. The weak positive correlation suggests that subjects with similar signal decompositions complete tasks in more time. This implies that the exact control input used is not a significant factor in the performance. As confirmation, the input similarities are compared with  $TP$ ,  $CT$  and  $PE$  values at the end of session 2, resulting in only weak relationships  $R = 0.08, 0.17, \text{ and } 0.41$ , respectively.

Mean completion time for all three precision tasks with sEMG was 30.6 minutes (95% CI [18.0, 43.1]). 7 subjects returned to establish a baseline performance time with keyboard inputs, which was 13.3 minutes (95% CI [7.2, 19.4]). While the significant difference ( $p = 0.01$ , paired student t-test) is expected due to the additional preparation time and familiarity with the tasks during the keyboard control, the best overall performance (6 minutes) was achieved by a subject with sEMG inputs. This subject is the only one in the study with significant video gaming experience. Clingman et. al [15] found that people with a background playing video games learn myoelectric control tasks much faster, perhaps due to enhanced ability to explore the potential input space. This, and the consistent learning trends shown by the other subjects, suggests that additional VR sessions may have allowed most subjects to perform similarly to the baseline completion time.

## IV. CONCLUSION

This work presents a novel motor learning-based control scheme to control a 7-DoF robotic arm and hand. A muscle synergy-inspired decomposition transforms HDsEMG into quasi-independent control inputs robust to slight electrode displacements and other external influences during long-term control. This decomposition removes constraints of targeted electrode placement while maintaining the session-independent benefits associated with motor learning. The control scheme produces simultaneous and proportional control of 4-DoFs in a two-state FSM offering both position and orientation control.

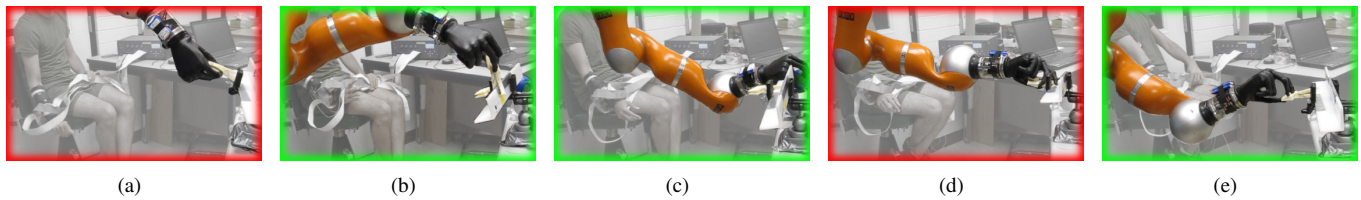


Fig. 7. Example chronological task sequence completed by a subject, with two examples of unsuccessful grasps (a and d) in red, and three successful grasps (b, c, e) in green, demonstrating the precision required to complete the tasks.

The study evaluates myoelectric motor learning from all healthy subjects through a practical control scheme designed for any general myoelectric interface. The performance of each subject in VR correlates with a sense of intuitive precision control with the robot. This implies that virtual interfaces may be used to implicitly train subjects to interact with a physical device. These findings may be significant for rehabilitation with amputees, as these motor learning principles may help them intuitively use functional prosthetic devices. This will be investigated in future work.

All subjects demonstrate learning trends consistent with typical motor skill learning, despite not knowing the control inputs nor non-intuitive mapping. The controls can be enhanced over time simply by interacting with the interface, similarly to learning a new motor skill. This learning, combined with the robust decomposition, offers robust long-term control desired in many myoelectric applications. The results confirm significant learning trends correlating with a feeling for more intuitive control, supporting this method as a potential alternative to pattern recognition for robust long-term control of myoelectric interfaces with enhanced functionality.

## REFERENCES

- [1] M. Ison and P. Artemiadis, "The role of muscle synergies in myoelectric control: trends and challenges for simultaneous multifunction control," *Journal of Neural Engineering*, vol. 11, no. 5, p. 051001, Oct 2014.
- [2] D. Farina, N. Jiang, H. Rehbaum, A. Holobar, B. Graimann, H. Dietl, and O. C. Aszmann, "The extraction of neural information from the surface emg for the control of upper-limb prostheses: Emerging avenues and challenges," *IEEE Transactions on Neural Systems and Rehabilitation Engineering*, vol. 22, no. 4, pp. 797–809, Jul 2014.
- [3] P. Artemiadis and K. Kyriakopoulos, "EMG-Based Control of a Robot Arm Using Low-Dimensional Embeddings," *Robotics, IEEE Transactions on*, vol. 26, no. 2, pp. 393–398, April 2010.
- [4] D. Tkach, A. Young, L. Smith, E. Rouse, and L. Hargrove, "Real-time and offline performance of pattern recognition myoelectric control using a generic electrode grid with targeted muscle reinnervation patients," *Neural Systems and Rehabilitation Engineering, IEEE Transactions on*, vol. 22, no. 4, pp. 727–734, July 2014.
- [5] J. Hahne, F. BieBmann, N. Jiang, H. Rehbaum, D. Farina, F. Meinecke, K.-R. Müller, and L. Parra, "Linear and nonlinear regression techniques for simultaneous and proportional myoelectric control," *Neural Systems and Rehabilitation Engineering, IEEE Transactions on*, vol. 22, no. 2, pp. 269–279, March 2014.
- [6] S. Muceli and D. Farina, "Simultaneous and proportional estimation of hand kinematics from emg during mirrored movements at multiple degrees-of-freedom," *Neural Systems and Rehabilitation Engineering, IEEE Transactions on*, vol. 20, no. 3, pp. 371–378, 2012.
- [7] N. Jiang, S. Dosen, K.-R. Müller, and D. Farina, "Myoelectric control of artificial limbs: is there the need for a change of focus?" *IEEE Signal Processing Magazine*, vol. 29, no. 5, pp. 149–152, 2012.
- [8] M. Ison, C. W. Antuvan, and P. Artemiadis, "Learning efficient control of robots using myoelectric interfaces," in *Robotics and Automation (ICRA), 2014 IEEE International Conference on*, May 2014, pp. 2880–2885.
- [9] N. Jiang, I. Vujaklija, H. Rehbaum, B. Graimann, and D. Farina, "Is accurate mapping of emg signals on kinematics needed for precise online myoelectric control?" *IEEE Transactions on Neural Systems and Rehabilitation Engineering*, vol. 22, no. 3, pp. 549–558, May 2014.
- [10] M. Ison and P. Artemiadis, "Proportional Myoelectric Control of Robots: Muscle Synergy Development drives Performance Enhancement, Retainment, and Generalization," *Robotics, IEEE Transactions on*, 2015 (in press).
- [11] M. Ison and P. Artemiadis, "Enhancing Practical Multifunctional Myoelectric Applications through Implicit Motor Control Training Systems," in *Engineering in Medicine and Biology Society (EMBC), International Conference of the IEEE*, 2014, pp. 3525–3528.
- [12] K. Nazarpour, A. Barnard, and A. Jackson, "Flexible Cortical Control of Task-Specific Muscle Synergies," *Journal of Neuroscience*, vol. 32, no. 36, pp. 12 349–12 360, Sep 2012.
- [13] T. Pistohl, C. Cipriani, A. Jackson, and K. Nazarpour, "Abstract and Proportional Myoelectric Control for Multi-Fingered Hand Prostheses," *Annals of Biomedical Engineering*, vol. 41, no. 12, pp. 2687–2698, Dec 2013.
- [14] C. W. Antuvan, M. Ison, and P. Artemiadis, "Embedded human control of robots using myoelectric interfaces," *IEEE Transactions on Neural Systems and Rehabilitation Engineering*, vol. 22, no. 4, pp. 820–827, Jul 2014.
- [15] R. Clingman and P. Pidcoe, "A novel myoelectric training device for upper limb prostheses," *Neural Systems and Rehabilitation Engineering, IEEE Transactions on*, vol. 22, no. 4, pp. 879–885, July 2014.
- [16] P. M. Fitts and M. I. Posner, *Human performance*. Brooks/Cole, 1967.
- [17] N. Jiang, K. B. Englehart, and P. A. Parker, "Extracting simultaneous and proportional neural control information for multiple-DOF prostheses from the surface electromyographic signal," *IEEE Transactions on Biomedical Engineering*, vol. 56, no. 4, pp. 1070–1080, Apr 2009.
- [18] S. Muceli, N. Jiang, and D. Farina, "Extracting signals robust to electrode number and shift for online simultaneous and proportional myoelectric control by factorization algorithms," *Neural Systems and Rehabilitation Engineering, IEEE Transactions on*, vol. 22, no. 3, pp. 623–633, May 2014.
- [19] F. E. Zajac, "Muscle and tendon: properties, models, scaling, and application to biomechanics and motor control," *Stanford University*, vol. 17, pp. 359–411, 1989.
- [20] J. M. Hahne, H. Rehbaum, F. Biessmann, F. C. Meinecke, K. Müller, N. Jiang, D. Farina, and L. C. Parra, "Simultaneous and proportional control of 2d wrist movements with myoelectric signals," in *Machine Learning for Signal Processing (MLSP), 2012 IEEE International Workshop on*, Sept 2012, pp. 1–6.
- [21] [Online]. Available: <http://www.opengi.org>
- [22] A. Simon, L. Hargrove, B. Lock, and T. Kuiken, "A Decision-Based Velocity Ramp for Minimizing the Effect of Misclassifications During Real-Time Pattern Recognition Control," *IEEE Transactions on Biomedical Engineering*, vol. 58, no. 8, pp. 2360–2368, Aug 2011.
- [23] R. W. Soukoreff and I. S. MacKenzie, "Towards a standard for pointing device evaluation, perspectives on 27 years of fitts' law research in hci," *Int. J. Hum.-Comput. Stud.*, vol. 61, no. 6, pp. 751–789, Dec. 2004.
- [24] M. R. Williams and R. F. Kirsch, "Evaluation of head orientation and neck muscle EMG signals as command inputs to a human-computer interface for individuals with high tetraplegia," *Neural Systems and Rehabilitation Engineering, IEEE Transactions on*, vol. 16, no. 5, pp. 485–496, Oct 2008.